Li^+ diffusion in the fast ionic conductor Li_3N investigated by beta -radiation detected NMR

1992 J. Phys.: Condens. Matter 4 4779

(http://iopscience.iop.org/0953-8984/4/20/005)

J. Phys.: Condens. Matter 4 (1992) 4779–4800. Printed in the UK

Li^+ diffusion in the fast ionic conductor Li_3N investigated by β-radiation detected NMR

B Bader†‡, P Heitjans†§, H-J Stöckmann†, H Ackermann†, W Buttler†||, P Freiländer†¶, G Kiese†‡‡, C van der Marel†§§ and A Schirmer†§|| ||

† Fachbereich Physik der Universität, Renthof 5, W 3550 Marburg, Federal Republic of Germany

Received 11 November 1991

Abstract. Applying the method of β-radiation detected nuclear magnetic resonance/relaxation (β-NMR) to ^8Li nuclei in $^7Li_3N$ single crystals comprehensive information on static and dynamic properties was obtained.

Below $T \simeq 200$ K the electric field gradients (EFG) at the two inequivalent Li lattice sites (Li(1), Li(2)) were determined. The spin–lattice relaxation (SLR) behaviour above $T \simeq 300$ K and the ^8Li NMR signals in the extreme narrowing regime ($T \geqslant 500$ K) could be attributed to interlayer diffusion involving Li^+ jumps between Li(1) and Li(2) lattice sites ((1↔2) jumps). In the temperature range 200 K $\leqslant T \leqslant$ 300 K the transients of the $^8Li(1)$ and $^8Li(2)$ polarizations were measured separately by applying a special radio-frequency scheme. The different SLR behaviour allowed us to study the Li^+ intralayer diffusion confined to the Li_2N layers. Furthermore, ultra-slow interlayer (1↔2) jumps with correlation times of up to 10 s were observed in this T region. Below 200 K a non-exponential ^8Li polarization decay depending weakly on B and T was observed. The SLR in this T range is discussed in terms of statistically distributed relaxation centres.

1. Introduction

Lithium nitride crystallizes in the hexagonal space group $P6/mmm$. The chemical bonding is ionic with the valence formula $(Li^+)_3N^{3-}$. The N^{3-} ion is coordinated by eight Li^+ ions occupying two different types of crystallographic sites. Six $Li^+(2)$ ions surround the N^{3-} ion in a hexagonal Li_2N plane and two $Li^+(1)$ ions are situated above and below this plane. The crystal structure can therefore be regarded as a layer structure with alternating Li_2N and pure Li layers (figure 1).

Li_3N is probably the ionic crystal most extensively studied in recent years. Earlier research was mainly concerned with the nature of chemical bonding [1–3], whereas

‡ Present address: Robert Bosch GmbH, W 6120 Erbach, Federal Republic of Germany.

§ Present address: Institut für Physikalische Chemie und Elektrochemie, Universität Hannover, Callinstrasse 3-3a, W 3000 Hannover, Federal Republic of Germany.

|| Present address: Auto-Meß GmbH, W 6802 Ladenburg, Federal Republic of Germany.

¶ Present address: Carl Freudenberg, W 6940 Weinheim, Federal Republic of Germany.

‡‡ Present address: Leybold-Heraeus GmbH, W 5000 Köln, Federal Republic of Germany.

§§ Present address: Philips, 5600 MD Eindhoven, The Netherlands.

|| || Also at: Institut für Festkörperforschung, KFA Jülich, W 5170 Jülich, Federal Republic of Germany.

0953-8984/92/204779+22$04.50

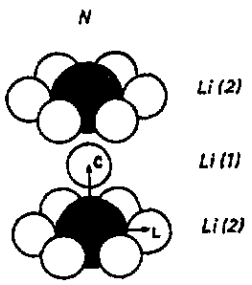

Figure 1. Crystal structure of Li_3N.

more recently a large variety of experimental techniques employing high-quality single crystals were used to explore a broad spectrum of static and dynamic properties (see e.g. [4] and references therein). Besides a concern in structural and electronic properties the main interest was in Li^+ diffusion, which turned out to be strongly anisotropic with conductivities $\sigma_{\parallel} \simeq 10^{-5}\ \Omega^{-1}\mathrm{cm}^{-1}$ and $\sigma_{\perp} \simeq 10^{-3}\ \Omega^{-1}\mathrm{cm}^{-1}$ parallel and perpendicular to the c-axis at room temperature [5]. Due to its high value of $\sigma_{\perp}$, Li_3N is ranked as a fast ionic conductor; its stability with respect to elemental Li initially promised its suitability for technical application as a solid electrolyte in lithium-based energy-storage systems [5]. Though this hope has not been fulfilled due to a rather low decomposition voltage of 0.44 V [4], Li_3N still attracts theoretical interest because it has some outstanding peculiarities:

(i) It has a relatively simple structure, with only four atoms per elementary cell, rendering it a model substance for studying anisotropic low-dimensional ionic diffusion and facilitating theoretical treatment.

(ii) In contrast to other fast ionic conductors Li_3N shows nearly complete ordering even at elevated temperatures [6]. So the generally accepted requirement for fast ionic conduction, namely dilute site occupation, is not fulfilled in the case of Li_3N .

(iii) It is the only compound where the existence of a N^{3-} ion, which is unstable as a free ion, has been proved [6].

(iv) It exhibits low-temperature acoustic and dielectric anomalies similar to those of amorphous materials [7].

This paper reports on β-radiation detected nuclear magnetic resonance/relaxation (β-NMR) studies using as probe nucleus the β emitter ^{8}Li ($T_{1/2} = 0.8$ s, $I = 2$) created by the neutron capture reaction $^7\mathrm{Li}(\vec{n},\gamma)^8\vec{\mathrm{Li}}$. This method has turned out to be a versatile microscopic tool in condensed matter research. For reviews see [8–11]. Some features of the β-NMR technique relevant to the present study are the following:

(i) The nuclear polarization produced by the capture of polarized thermal neutrons, which is purely dipolar, is independent of any Boltzmann factor. Thus, measurements in low external magnetic fields and at high temperatures do not suffer from reduced sensitivity. In fact, the present β-NMR measurements extend to considerably lower fields and Larmor frequencies than previous NMR studies of Li_3N. As far as spin–lattice relaxation (SLR) is concerned this allows one to study slow-motional processes with long correlation times [10].

(ii) The concentration of the neutron activated probes is extremely small (typically 10^{-18}) and there is no homonuclear spin coupling. Consequences here are,

among others, that ^{8}Li nuclei at inequivalent sites keep their individual relaxation behaviour and that paramagnetic impurities beyond the near ^{8}Li neighbourhood do not contribute to spin–lattice relaxation.

(iii) In measuring a SLR time no radio-frequency field is required. In the present context this implies, e.g., that the relaxation of either of two ^{8}Li spin species at inequivalent sites can easily be studied while the polarization of the other is destroyed by selective radio-frequency irradiation.

The β-NMR measurements on Li_3N are in several respects complementary to those of conventional NMR on the stable isotopes ^{6}Li and ^{7}Li, which contributed decisively to the clarification of the diffusion processes in Li_3N [12–14]. Thus, being able to employ three Li isotopes with different magnetic dipole and electric quadrupole moments yields detailed information on the magnetic and electric interactions of the Li probe nuclei and allows an examination of models used to describe the Li motion. Other aspects of β-NMR are useful and were successfully utilized to obtain supplementary information hardly accessible by conventional NMR. So, e.g., the individual polarizations of ^{8}Li(1) and ^{8}Li(2) nuclei could be measured separately as indicated above and interlayer diffusion in the ultra-slow motion regime with correlation times as long as 10 s could be observed. Furthermore the magnetic field and temperature dependence of the inhomogeneously averaged spin–lattice relaxation time T_{1inh} below $T = 160$ K led to an interpretation in the sense of fluctuating defect centres.

2. Experimental details

The experiments were performed at the high flux reactor of the ILL in Grenoble using the in-beam NMR spectrometer S6. Polarized β-active ^{8}Li nuclei were produced in the $^7Li_3N$ single crystals by capture of polarized thermal neutrons. The flux was 5×10^7 cm^{-2} s^{-1} and the degree of polarization about 95%. The ^{8}Li polarization P was monitored via the asymmetry of the β radiation with respect to the external magnetic field B. P was measured either in a time-integral way with continuous neutron activation in order to observe NMR spectra or in a time-differential way with pulsed neutron activation, which allows direct determination of SLR times (see [9] for details).

We used two Li_3N single crystals grown by the Czochralski method [15] with 99.9 % isotopically pure ^{7}Li. They were kindly put at our disposal by the Max-Planck-Institut für Festkörperforschung in Stuttgart. During crystal growth it is inevitable that small amounts of hydrogen enter the probe. The relative H contents were determined by infrared absorption measurements in the wave number range $\kappa = 3100, \ldots, 3150$ cm^{-1}. Several sharp absorption lines were observed, these being attributed to vibrations of $(NH)^{--}$ ions. Thus the integral over the absorption coefficient is proportional to the hydrogen concentration. According to an estimation given in [16] for our samples we obtained H concentrations $n_H \simeq 6 \times 10^{19}$ cm^{-3} and $n_H \simeq 3 \times 10^{20}$ cm^{-3}, respectively.

3. ^{8}Li nuclear magnetic resonance

3.1. Quadrupolar-split ^{8}Li NMR spectra

The hexagonal crystal structure of Li_3N leads to axially symmetric electrical field gradients (EFG) at the regular Li lattice sites Li(1) and Li(2) (see figure 1) with the principal axes parallel to the c direction. In an external magnetic field B the interaction of these EFGs with the quadrupole moments of the ^{8}Li nuclei ($Q = 3.2 \times 10^{-30}$ m^2) residing on a Li(1) or Li(2) position results in a quadrupolar-split NMR spectrum containing two sets of four resonance lines. In first-order perturbation theory ($\nu_L \gg e^2qQ/h$) the frequencies are given by

$$\nu_{m,m-1}(i) = \nu_L + \frac{1}{16}\frac{e^2q(i)Q}{h}(3\cos^2\theta - 1)(2m-1)$$
$$m = 2, \ldots, -1 \qquad i = 1, 2 \tag{1}$$

with ν_L the Larmor frequency, $eq(i)$ the EFG at a Li(i) position and θ the angle between the c-axis and the direction of B.

The spectrum can be measured by applying a radio frequency (RF) field $B_1(t) = B_1 \cos(2\pi\nu t)$ perpendicular to the external field B. If the condition $\nu = \nu_{m,m-1}(i)$ is fulfilled the time-averaged polarization $P(i)$ of the ^{8}Li(i) ensemble is reduced by only 5 %, assuming complete saturation [17]. In order to get a better signal to noise ratio we used a special resonance enhancement technique, which consists in irradiating four RF fields, one to scan the line $\nu_{m,m-1}(i)$ under study and three with fixed frequencies $\nu_{m',m'-1}(i)(m' \neq m)$ to saturate the adjacent transitions simultaneously. In this way the signal to noise ratio is augmented by a factor of 10 if ν is swept over one of the outer satellites $\nu_{2,1}(i)$ or $\nu_{-1,-2}(i)$ and by a factor of 15 in the case of the inner satellites $\nu_{1,0}(i)$ or $\nu_{0,-1}(i)$. From the positions of the resonance lines in figure 2 the absolute values of the quadrupole coupling constants (QCC) $|e^2q(1)Q/h| = 441(3)$ kHz and $|e^2q(2)Q/h| = 212(3)$ kHz were obtained.

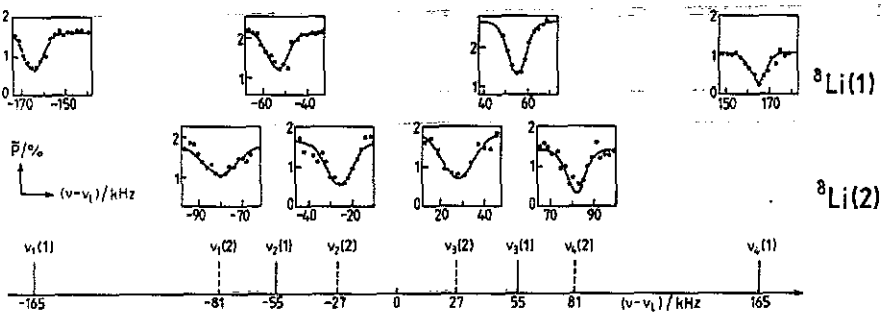

Figure 2. Quadrupolar-split NMR spectrum of ^{8}Li in $^7Li_3N$ at $T = 9$ K, $B \parallel c$. In order to enhance the resonance depth of an investigated line, adjacent transitions were saturated additionally (see text for details).

The assignment of q(1) to Li(1) and q(2) to Li(2) could be proved by inspecting the depths of the resonance lines, which for the more abundant ^{8}Li(2) spin ensemble turned out to be nearly a factor of two larger.

The accuracy in the determination of $e^2q(i)Q/h$ was improved by measuring, in addition, the integral lineshape [17] and two-quanta transitions [18] resulting in

$$|e^2q(1)Q/h| = 445(1)\ \text{kHz} \qquad |e^2q(2)Q/h| = 216(1)\ \text{kHz}. \tag{2}$$

The absolute values of the EFGs $|eq(1)|$ and $|eq(2)|$ are slightly smaller than those determined by classical NMR on ^{7}Li [12, 19], which is probably due to a slight misorientation ($\theta \simeq 6°$) of our crystal (see table 1). Both methods are in exact accordance concerning the orientation-independent ratio $|eq(1)/eq(2)|$: classical NMR yields $|eq(1)/eq(2)| = 2.04(2)$ and β-NMR $|eq(1)/eq(2)| = 2.06(2)$.

Table 1. Electric field gradient values $eq(i)$ in 10^{20} V m^{-2}.

	$eq(1)$	$eq(2)$	$eq(1)/eq(2)$
Experiment			
β-NMR (^{8}Li)	$\pm 5.76(7)$[a]	$\mp 2.80(4)$[a]	−2.06(2)
class. NMR (^{7}Li)	$\pm 5.87(2)$	$\mp 2.88(2)$	−2.04(2)
Theory			
LAPW[b]	−6.94	+3.41	−2.04

[a] The standard deviation is given by the inaccuracy of the quadrupole moment $Q(^8\text{Li})$.
[b] Linear augmented plane wave.

The signs of the EFGs are not determinable with methods creating and detecting purely dipolar polarizations [8]. The sign of the ratio $eq(1)/eq(2)$, however, could be determined by virtue of a special Li-diffusion process (interlayer diffusion), as will be shown in section 3.2, and proved to be negative. Self-consistent energy-band calculations using the linear augmented plane wave (LAPW) method [20] yielded $eq(1) > 0$ and $eq(2) < 0$. The measured EFG values were reproduced within an accuracy of about 20 %. Within the framework of these calculations a large contribution to the EFGs is due to local distortions of the electronic charge density, especially in the case of the polarizable N^{3-} ion. Thus the assumption of ionic bonding in Li_3N consisting of Li^+ and N^{3-} ions is corroborated by the NMR results.

3.2. *The influence of diffusion processes on the ^{8}Li NMR spectrum*

The shapes of the ^{8}Li(1)- and ^{8}Li(2)-NMR spectra measured in the rigid Li_3N lattice remain unaltered up to a temperature of $T \simeq 220$ K. Between 220 K and 280 K the linewidths decrease. Above $T \simeq 280$ K a broadening sets in, which can be pursued up to $T \simeq 350$ K. In the T range $350\ \text{K} \leqslant T \leqslant 470$ K no spectra can be observed as spin–lattice relaxation becomes so fast that P vanishes. Above $T \simeq 470$ K a new spectrum appears containing four resonance lines with a drastically reduced quadrupole coupling constant (figure 3).

These changes can be understood by two Li-diffusion processes: (i) intralayer diffusion perpendicular to the c-axis and (ii) interlayer diffusion parallel to the c-axis consisting of Li^+ jumps between Li(1) and Li(2) lattice sites ((1↔2) jumps). We shall not discuss the T dependence of the ^{8}Li linewidths in detail here and shall only mention that the intralayer diffusion causes the motional narrowing in the range $220\ \text{K} \leqslant T \leqslant 280$ K, whereas the subsequent broadening can be explained by slow

(1↔2) jumps (interlayer diffusion). This broadening is, in a way, a lifetime broadening which sets in when the mean residence time $\tau_{\parallel}(i)$ of a ^{8}Li nucleus on a Li(i) site becomes smaller than the inverse line width. From the linewidths in this T region (1↔2) jump rates can be determined (see figure 9). For further details we refer to [21].

The high-temperature spectrum in figure 3 comes about by a motional narrowing process due to the interlayer diffusion. The quadrupole moment of a probe nucleus jumping between Li(1) and Li(2) sites interacts with a time dependent EFG which takes the values $eq(1)$ and $eq(2)$ at a random rate. As soon as the (1↔2) jump rate exceeds the spacing of two corresponding resonance frequencies, i.e. $2\pi|\nu_{m,m-1}(1)-\nu_{m,m-1}(2)|$, an averaging sets in and the static coupling constants $e^2q(1)Q/h$ and $e^2q(2)Q/h$ must be replaced by the weighted mean value

$$e^2\bar{q}Q/h = \tfrac{1}{3}e^2q(1)Q/h + \tfrac{2}{3}e^2q(2)Q/h. \tag{3}$$

This narrowing process showed up earlier in conventional NMR on ^{7}Li [14]. At $T = 550$ K we measured

$$|e^2\bar{q}Q/h| = 2.0(3)\ \text{kHz}. \tag{4}$$

Within a model of well defined (1↔2) jumps this small QCC is only understandable if the static field gradients $eq(1)$ and $eq(2)$ have opposite signs. Then with the values (2) we obtain

$$|e^2\bar{q}Q/h| = 4(1)\ \text{kHz}. \tag{5}$$

The agreement with (4) is not exact as the values of the static coupling constants stem from measurements carried out at much lower temperatures. Actually $e^2\bar{q}Q/h$ decreases strongly with temperature, which can be explained by the different T dependences of $e^2q(1)Q/h$ and $e^2q(2)Q/h$ due to the anisotropic thermal expansion of the Li_3N crystal [14].

The function used to fit the lineshape of the ^{8}Li NMR spectrum in figure 3 stems from an exact calculation including the RF irradiation and assuming stochastic jumps between the two sites.

That the EFG signs are opposite can be proved by a more direct method, which works in the temperature range 250 K $\leqslant T \leqslant$ 325 K, where the (1↔2) jump rates are of the order of the inverse β lifetime τ_β^{-1}, so the ^{8}Li spectra of the rigid lattice are effective. Here it is possible to determine the relative signs of the EFGs by appropriate irradiation of Li(1) and Li(2) resonance frequencies. The experimental results show again that $eq(1)/eq(2) < 0$ holds (for details see [22]).

4. ^{8}Li spin lattice relaxation (SLR)

4.1. Synopsis

A survey of the overall temperature dependence of the ^{8}Li SLR rate T_1^{-1} is given in figure 4. The ^{8}Li transients behave differently in the three indicated T ranges. In T range I a single-exponential polarization decay is observed, which becomes significantly two-exponential in T range II (figure 7). In this regime the ^{8}Li(1) and ^{8}Li(2) nuclei relax single-exponentially but with different SLR times as will be shown later in section 4.3.1. Finally, in T range III non-exponential SLR shows up with a common time constant for both spin ensembles.

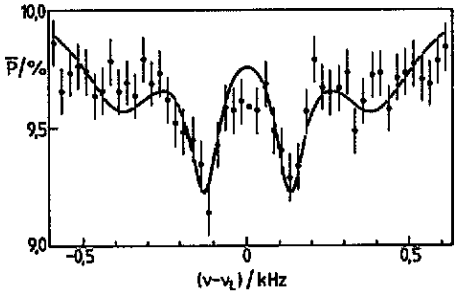

Figure 3. Quadrupolar-split spectrum of ^{8}Li resulting from motional averaging of the spectra shown in figure 2. $T = 650$ K, $B = 301.8$ mT, $B \parallel c$, correlation time $\tau_\parallel = 1.5 \times 10^{-9}$ s (from T_1 measurements), fit parameters: $|e^2\bar{q}Q/h| = 1.0(1)$ kHz, RF field strength $B_1 = 0.53(5)$ μT, for fit function see text.

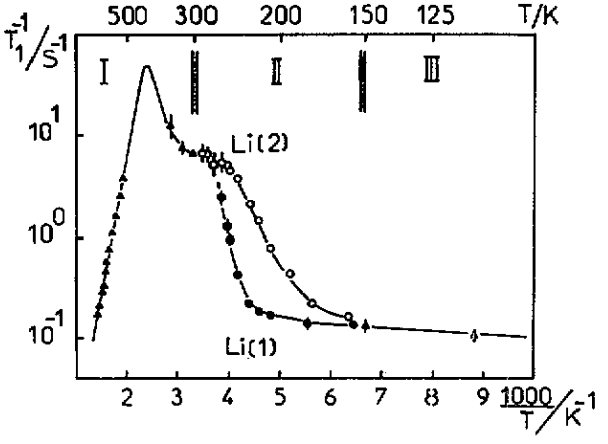

Figure 4. Temperature dependence of ^{8}Li SLR in Li_3N (hydrogen-rich sample, $n_H \simeq 3 \times 10^{20}$ cm^{-3}) at $B = 300$ mT, $\theta \simeq 15°$. Circles: T_1^{-1} determined from the individual transients $P(1)(t)$ and $P(2)(t)$, triangles: T_1^{-1} determined from the total transient $P(t)$ by single-exponential fits.

4.2. ^{8}Li SLR in the temperature range I ($T > 300$ K)

4.2.1. Measurements. The T_1^{-1} peak (figure 4) suggests a thermally activated process. From the high-temperature slope an activation energy of 570 meV can be inferred, which is identical to that obtained from ionic conductivities $\sigma_\parallel$ parallel to the c-axis [5, 16, 23]. The process governing the ^{8}Li SLR in this region is thus interlayer diffusion. Furthermore, a strong orientational dependence of T_1^{-1} is observed (figure 5) indicating extremely anisotropic interactions to be involved in the relaxation process. In order to measure the SLR over the whole T range I, it is convenient to orient the Li_3N crystal with its c-axis nearly parallel to B_+ since otherwise T_1 becomes too short with respect to τ_β and can no longer be measured (see e.g. [9]). Figure 6 shows the T dependence for the orientation $\theta \simeq 5°$. Fitting the data with the (simplified) formula of Bloembergen *et al* (BPP) [24]

$$T_1^{-1} \sim 2\tau_\parallel/(1 + \omega_L^2\tau_\parallel^2) \tag{6}$$

and assuming an Arrhenius relation $\tau_{\parallel} = \tau_{0\parallel}\exp(E_{\parallel}/kT)$ for the correlation time $\tau_{\parallel}$ of the interlayer diffusion we obtained

$$E_{\parallel} = 590(30)\ \text{meV} \qquad \tau_{0\parallel} = 10^{-14(0.5)}\ \text{s} \tag{7}$$

for the hydrogen-poor sample and

$$E_{\parallel} = 570(20)\ \text{meV} \qquad \tau_{0\parallel} = 10^{-14(0.5)}\ \text{s} \tag{8}$$

for the hydrogen-rich sample. For the fitting procedure, only the data on the high-T side of the T_1^{-1} maximum were taken into account. The deviations on the low-temperature side are due to the influence of the intralayer diffusion. Subtracting the BPP fit result (dashed line in figure 6) from the measured values we obtain the dotted smoothed curve, which roughly reflects the contribution of the intralayer diffusion to the ^{8}Li SLR.

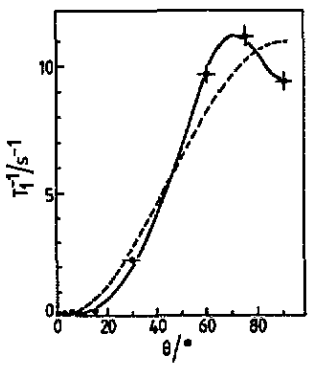

Figure 5. Orientational dependence of ^{8}Li SLR in Li_3N (hydrogen-poor sample, $n_H \simeq 6\times10^{19}\,cm^{-3}$) at $T = 715$ K, $B = 300$ mT. Solid line: fit according to (14), broken line: fit according to $T_1^{-1} \propto \sin^2\theta$

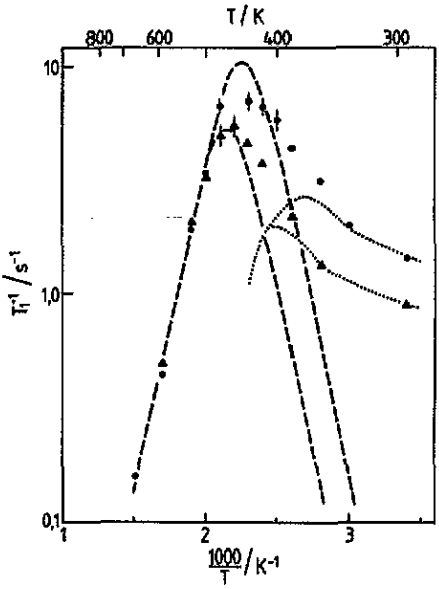

Figure 6. Temperature dependence of ^{8}Li SLR in Li_3N (hydrogen-poor sample) at $\theta \simeq 5°$ in T range I. Dots: $B = 300$ mT, triangles: $B = 600$ mT, broken line: BPP fit according to (13), dotted line: T_1^{-1} contribution of the intralayer diffusion

4.2.2. Discussion. The experimental results of the previous section can be unambigously interpreted by a Li^+ jump process between Li(1) and Li(2) lattice sites as was confirmed earlier by Brinkmann *et al* [13]. A probe nucleus jumping rapidly between lattice sites with different field gradients undergoes quadrupolar SLR. For $I = 2$ the polarization decay will be two-exponential (equation (A.8) in [25]).

$$P(t) = P_0[a_s\exp(-\lambda_s t) + a_f\exp(-\lambda_f t)]. \tag{9}$$

The fast and the slow relaxation rates are given by

$$\lambda_{f/s} = [(eQ/\hbar)^2/32]\left(13J_1 + 16J_2 \pm \sqrt{145J_1^2 + 64J_2^2 + 16J_1J_2}\right) \tag{10}$$

where $J_1 = J_1(\omega_L)$ and $J_2 = J_2(2\omega_L)$ are the spectral density functions of the fluctuating quadrupolar interaction. The prefactors $a_{f,s}$, which depend on the spectral densities J_1 and J_2, obey the relation $a_f/a_s \leqslant 1/5$ for a purely dipolar polarization [21]. It will thus be sufficient to describe the ^{8}Li transients by single-exponential functions

$$P(t) \simeq P_0 \exp(-t/T_1) \tag{11}$$

where the relaxation rate T_1^{-1} is equal to λ_s.

A calculation of the spectral density functions $J_m(m\omega_L)$ of the interlayer diffusion is performed in the appendix, yielding

$$\begin{aligned} J_1(\omega_L) &= \tfrac{1}{12}[eq(1) - eq(2)]^2 \sin^2\theta \cos^2\theta \frac{2\tau_\parallel}{1+\omega_L^2\tau_\parallel^2} \\ J_2(2\omega_L) &= \tfrac{1}{48}[eq(1) - eq(2)]^2 \sin^4\theta \frac{2\tau_\parallel}{1+4\omega_L^2\tau_\parallel^2}. \end{aligned} \tag{12}$$

In [13], instead of the factor $[eq(1) - eq(2)]^2$ in equation (12), the factor $\frac{3}{2}[eq(1)^2 + 2eq(2)^2]$ was given. This has since been corrected [26]. By accident both expressions yield about the same numerical values, because $eq(1) \simeq -2eq(2)$ holds for Li_3N. The correlation time $\tau_\parallel$ is given by $1/\tau_\parallel = 1/\tau_\parallel(1) + 1/\tau_\parallel(2)$, where the $\tau_\parallel(i)$ are the mean residence times of a ^{8}Li nucleus on a given Li(i) site. From the law of detailed balance we also have $\tau_\parallel(2)/\tau_\parallel(1) = 2$ corresponding to the number ratio $N(2)/N(1) = 2$ of ^{8}Li(2) to ^{8}Li(1) nuclei. In this description we neglected possible spatial and temporal correlations of the (1↔2) jump process.

In figure 6 the T dependence of T_1^{-1} was fitted with a BPP formula (6). For an orientation close to $B \parallel c$, (10) and (12) do indeed yield a simple BPP formula

$$T_1^{-1} = 0.96(\pi^2/96)\Delta C^2\theta^2 2\tau_\parallel/(1+\omega_L^2\tau_\parallel^2) \tag{13}$$

where $\Delta C = e^2q(1)Q/h - e^2q(2)Q/h$. This justifies the use of (6) to fit the T dependences shown in figures 4 and 6.

The correctness of the (1↔2) jump model can be verified decisively by the orientational dependence of the SLR rate, which was measured at $T = 715$ K (figure 5). At this temperature we have $\omega_L\tau_\parallel \ll 1$. Inserting (12) into (10) one gets

$$T_1^{-1} = (\pi^2/48)\Delta C^2\tau_\parallel \sin^2\theta[13 - 9\sin^2\theta - \sqrt{145(1+\sin^4\theta) - 286\sin^2\theta}]. \tag{14}$$

The continuous line in figure 5 represents a fit with this formula.

Quadrupolar SLR is often interpreted by means of the simple formula

$$T_1^{-1} = \frac{3}{20}\frac{2I+3}{I^2(2I-1)}\left(\frac{eQ}{\hbar}\right)^2[J_1(\omega_L) + 4J_2(2\omega_L)] \tag{15}$$

which holds in the special case of a spin system having a common spin temperature. In more general cases this is a fairly good approximation of the relatively complicated expression (10) for λ_s as long as $J_1(\omega_L) \simeq J_2(2\omega_L)$. Inserting the spectral densities (12) here we get an orientational dependence $1/T_1 \sim \sin^2\theta$, which was also fitted to the data of figure 5 (dashed line). Excellent agreement of (14) with the $1/T_1(\theta)$ values is obtained, whereas the simple $1/T_1 \sim \sin^2\theta$ behaviour yields an insufficient fit. The fit result $\Delta C^2\tau_{\parallel} = 23(1)\ s^{-1}$ together with the values of $\tau_{\parallel}$ and $E_{\parallel}$ from (8) lead to $|\Delta C| = |e^2q(1)Q/h - e^2q(2)Q/h| = 400(200)$ kHz, which has to be compared with $|\Delta C| = 660(3)$ kHz obtained from the ^{8}Li NMR signals at low temperatures. The large error in the first value is due to the uncertainty of the Arrhenius prefactor $\tau_{0\parallel}$. The agreement of the two values is, however, satisfactory.

The orientational dependence of T_1^{-1} thus confirms the following:

(i) The model of the (1↔2) jumps for the interlayer diffusion.

(ii) The functional depedence of the slow relaxation rate λ_s on the spectral densities $J_1(0)$ and $J_2(0)$ according to equation (10).

(iii) The lack of spin temperature for the ^{8}Li spin ensemble.

The quadrupolar nature of the SLR can be verified by comparing T_1^{-1} values of ^{8}Li and ^{7}Li. For this purpose it is convenient to choose $\theta = 90°$, because possible misorientations of the crystal then cause only slight variations of T_1. In this case, a ratio of

$$\frac{T^{-1}(^8\mathrm{Li}, 90°)}{T^{-1}(^7\mathrm{Li}, 90°)} = \tfrac{1}{4}(Q_8/Q_7)^2 = 0.15 \tag{16}$$

is expected on the high-T side ($\omega_L\tau_{\parallel} \ll 1$). A comparison of our measurements with those of Brinkmann *et al* [13] yields the ratio 0.16(1). This proves that the interlayer diffusion does indeed give rise to quadrupolar relaxation.

A further point of interest is the lack of H impurity influence on the ^{8}Li SLR. For both the hydrogen-poor sample and the hydrogen-rich sample the same activation energies and Arrhenius prefactors were obtained (7),(8). A similar behaviour was observed in the ionic conductivity $\sigma_{\parallel}$ [16] which changed insignificantly if the H concentration was varied by a factor of 15. Thus it can be concluded that the defect type 'NH^{--} dipole plus Li(2) vacancy', assumed for Li_3N, does not play an important role for the interlayer diffusion. It seems more probable that the diffusion process is realized by thermally activated vacancies at the Li(1) and Li(2) sites.

4.3. ^{8}Li SLR in the temperature range II (300 K ≥ T ≥ 180 K)

Here we mainly used the hydrogen-rich Li_3N crystal. The high hydrogen content compared with that of the hydrogen-poor sample causes a shift of the $1/T_1$ maximum induced by the intralayer diffusion (dotted line in figure 6) to lower temperatures, thus leading to a better separation of this SLR mechanism from that brought about by the interlayer diffusion. This is in agreement with measurements of the ionic conductivity $\sigma_{\perp}$, which is enhanced with increasing H concentration [16].

4.3.1. The ^{8}Li transients. Below $T = 300$ K the ^{8}Li transients become clearly non-exponential. An example is shown in figure 7, where a sum of two exponentials is fitted to the data. Here the ^{8}Li(1) and ^{8}Li(2) nuclei relax single-exponentially but with different SLR times. This was proved in the following way. The polarization of one of

the two spin ensembles, i.e. $P(1)$ or $P(2)$ was destroyed during a T_1 measurement by irradiating the four resonance frequencies of the corresponding quadrupolar-split spectrum (see figure 2). One is then left with the polarization of the other ^{8}Li spin species. The transients $P(1)(t)$ and $P(2)(t)$ measured in this way were single-exponential, with SLR times $T_1(i)$ near the values $\tilde{T}_1(i)$, given in figure 7. As T_1 values inferred from two-exponential fits are in general only reliable if the difference between the two time constants is large (this is the case in figure 7, where $\tilde{T}_1(1)/\tilde{T}_1(2) \simeq 15$) the RF-separation method was used over the whole T range II.

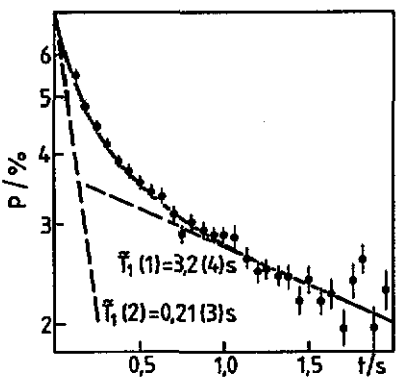

Figure 7. ^{8}Li transient (hydrogen-rich sample) at $T = 239$ K, $B = 300$ mT and $\theta \simeq 15°$. A sum of two exponentials (continuous line) with relaxation times $\tilde{T}_1(1)$, $\tilde{T}_1(2)$ was fitted to the data.

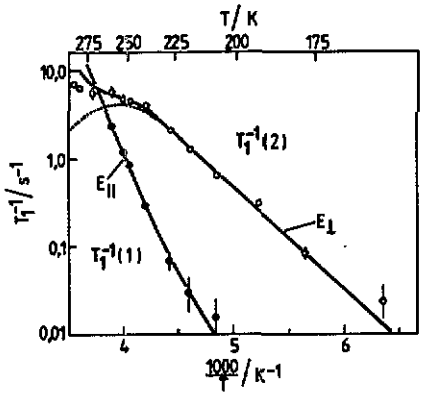

Figure 8. Temperature dependence of the ^{8}Li SLR rates, determined from the individual transients $P(i)(t)$. For the hydrogen-rich sample, $B = 300$ mT, $\theta \simeq 15°$. Solid line: fit according to $T_1^{-1}(i) = R_\perp(i) + \tau_\parallel^{-1}(i)$ (see equations (21), (22)), dotted line: contribution of $R_\perp(2)$ to $T_1^{-1}(2)$.

4.3.2. The influence of slow (1↔2) jumps on SLR. Between $T \simeq 180$ K and $T \simeq 250$ K the correlation time $\tau_\parallel$ is of the order of 1 s, so that the spectral densities depend only on the correlation time $\tau_\perp$ of the intralayer diffusion, which is of the order of 10^{-6} s. The slow (1↔2) jumps, however, transfer polarization between the two spin ensembles, which modifies the SLR times. This influence is treated in the following way (see also [22]).

We assume that without (1↔2) jumps the intralayer diffusion leads to single-exponential individual transients

$$P(i)(t) = P_0 \exp[-R_\perp(i)t] \qquad i = 1, 2 \tag{17}$$

with the frequency- and temperature-dependent SLR rates $R_\perp(i)$. For the present we do not make an assumption about their functional dependences. The polarization transfer due to the slow (1↔2) jumps is taken into consideration by the following master equation

$$\begin{aligned} \dot{P}(1) &= -[R_\perp(1) + \tau_\parallel^{-1}(1)]P(1) + \tau_\parallel^{-1}(2)P(2) \\ \dot{P}(2) &= \tau_\parallel^{-1}(1)P(1) - [R_\perp(2) + \tau_\parallel^{-1}(2)]P(2). \end{aligned} \tag{18}$$

For the total polarization $P(t) = P(1)(t) + P(2)(t)$ we get from these equations

$$P(t) = \tilde{P}_0(1)\exp[-t/\tilde{T}_1(1)] + \tilde{P}_0(2)\exp[-t/\tilde{T}_1(2)] \tag{19}$$

with the relaxation rates

$$1/\tilde{T}_1(1,2) = (1/2)\Big(R_\perp(1) + R_\perp(2) + (1/\tau_\parallel) \mp \sqrt{[R_\perp(1) - R_\perp(2) + (1/3\tau_\parallel)]^2 + \tfrac{8}{9}(1/\tau_\parallel^2)}\Big) \tag{20}$$

where the relation $1/\tau_\parallel = 1/\tau_\parallel(1) + 1/\tau_\parallel(2)$ was used. The prefactors $\tilde{P}_0(i)$ depend on $R_\perp(i)$, $\tau_\parallel$ and the initial polarizations $P_0(i)$. It should be mentioned that for $1/\tau_\parallel \to \infty$ the system relaxes single-exponentially with the weighted average rate $1/\tilde{T}_1 = 1/3R_\perp(1) + 2/3R_\perp(2)$. The relaxation behaviour becomes much simpler in the case of selective RF irradiation. Then, from (18), setting $P(2) = 0$ or $P(1) = 0$ we immediately get

$$\begin{aligned} &P(t) = P(i)(t) = P_0(i)\exp[-t/T_1(i)] \qquad i = 1,2 \\ &1/T_1(i) = R_\perp(i) + 1/\tau_\parallel(i). \end{aligned} \tag{21}$$

Subtracting the T_1^{-1} values extrapolated from T range III beyond $T = 180$ K we get the relaxation rates $1/T_1(1)$ and $1/T_1(2)$ shown in figure 8. In order to determine the contributions $R_\perp(1)$, $R_\perp(2)$ and $\tau_\parallel$ we use, as a starting point,

$$R_\perp(i) = a_\perp(i)\frac{\tau_\perp}{1+\omega_L^2\tau_\perp^2} \qquad \tau_\perp = \tau_{0\perp}e^{E_\perp/kT} \qquad \tau_\parallel = \tau_{0\parallel}e^{E_\parallel/kT}. \tag{22}$$

It should be mentioned here that the BPP *ansatz* for $R_\perp(i)$ does not appropriately describe the measured ω dependence (see figure 10). It should, thus, be treated as a spline function, which for a fixed frequency ω_L reproduces the temperature dependence of $R_\perp(1)$ and $R_\perp(2)$ satisfactorily . Fitting the $1/T_1(i)$ data in figure 8 with (21) and (22) one obtains

$$\begin{aligned} &a_\perp(2)/a_\perp(1) \simeq 100 \\ &E_\perp = 240(30)\ \text{meV} \qquad E_\parallel = 565(30)\ \text{meV} \\ &\tau_{0\perp} = 10^{-12(0.5)}\ \text{s} \qquad \tau_{0\parallel} = 10^{-12(0.5)}\ \text{s}. \end{aligned} \tag{23}$$

Equations (23) can be interpreted as follows:

(i) *Confinement of the intralayer diffusion to the Li_2N layers.* The large ratio $a_\perp(2)/a_\perp(1) = R_\perp(2)/R_\perp(1)$ means that the intralayer diffusion depolarizes the ^{8}Li(2) nuclei preferentially and has practically no influence on the ^{8}Li(1) polarization. The ionic motion perpendicular to the c-axis in T range II is therefore restricted to the Li_2N layers involving Li(2) ions only. This result is in accordance with ^{7}Li linewidth measurements [14], where the motional narrowing for the ^{7}Li(2) nuclei is much stronger than that for the ^{7}Li(1) nuclei. For $T \leqslant 250$ K the contribution $1/\tau_\parallel(2)$ is negligible compared to $R_\perp(2)$, i.e. $1/T_1(2) \simeq R_\perp(2)$. The absolute value of the slope in figure 8 (open circles) is therefore equal to $E_\perp$.

(ii) *Direct measurement of* $\tau_{\parallel}(1)$ *via* $P_1(t)$. For $T \geqslant 230$ K the contribution $R_{\perp}(1)$ is negligible compared to $1/\tau_{\parallel}(1)$, i.e. $T_1(1) \simeq \tau_{\parallel}(1)$. A ^{8}Li nucleus residing initially at a Li(1) lattice site is depolarized after the mean residence time $\tau_{\parallel}(1)$, when it jumps to a Li(2) lattice site, where it is sensitive to the resonant RF radiation. The slope in figure 8 (filled cirles) therefore shows the activation energy $E_{\parallel}$ of the (1↔2) jumps. We note that ultra-slow jump rates corresponding to $\tau_{\parallel}(1) \simeq 10$ s have been determined by these SLR measurements.

Further experimental tests of the present model are measurements of $T_1^{-1}(1)$ as a function of B and θ. Obviously neither a B nor a θ dependence should occur at temperatures, where $T_1(1) = \tau_{\parallel}(1)$ is valid, as $\tau_{\parallel}(1)$ only depends on T via the Arrhenius law. This was verified experimentally for 100 mT $\leqslant B \leqslant$ 500 mT and the orientations $\theta \simeq 15°$ and $\theta = 90°$ [27].

4.3.3. The T dependence of $1/\tau_{\parallel}$. The T dependence of the correlation rate $1/\tau_{\parallel}(T)$ determined by β-NMR, classical NMR and ionic conductivity is shown in figure 9. The β-NMR method yielded $\tau_{\parallel}$ in three different time windows. The first is located near the Larmor precession time $1/\omega_L$ for the SLR measurements in T range I, the second near the inverse ^{8}Li linewidth $\Delta\omega^{-1}$ for the linewidth measurements briefly mentioned in section 3.2 and the third near the lifetime τ_β for the individual transients $P(1)(t)$ (this section).

The ionic conductivity $\sigma_{\parallel}$ can be converted into $1/\tau_{\parallel}$ by use of the Nernst–Einstein relation

$$\sigma_{\parallel} = D_{\parallel} q^2 n / kT \tag{24}$$

with the diffusion constant $D_{\parallel} = c^2/2\tau_{\parallel}$, where c is the projection of the (1↔2) jump vector on the c-axis. q and n are the charge and concentration, respectively, of the Li ions ($n = 6.56 \times 10^{22}$ cm^{-3}).

Strictly speaking, SLR and ionic conductivity do not yield the same $\tau_{\parallel}$ due to their different sensitivities to spatial and temporal correlations of the diffusion process. As these differences are in general small it is not necessary to make a distinction between $\tau_{\parallel}$, $\tau_{\parallel}^{\sigma}$ and $\tau_{\parallel}^{NMR}$ in view of the measuring accuracy.

As the NMR and $\sigma_{\parallel}$ measurements yield about the same correlation times (see figure 9), the diffusion along the c-axis is principally due to the (1↔2) jumps. Schulz and Thiemann [6] and Nishida *et al* [28] attribute interlayer diffusion to Li(2)–Li(2) jumps between different Li_2N layers. These jumps would not yield an appreciable contribution to SLR, as only equivalent lattice sites are involved. The ionic conductivity $\sigma_{\parallel}$, however, would be sensitive to these additional jumps and would yield a different activation energy $E_{\parallel}$ and larger $\tau_{\parallel}^{-1}$ values.

4.3.4. The ^{8}*Li(2) SLR rate* $R_{\perp}(2)$ *induced by intralayer diffusion.* The activation energy $E_{\perp}$ was determined from the slope of $T_1^{-1}(2) \simeq R_{\perp}(2)$ (figure 8) assuming a BPP spectral density (22), which predicts $T_1 \propto B^2$ on the low-T slope (LTS). The relaxation time $T_1(2)$, however, obeys the empiric formula $T_1(2) \propto B^{\alpha}$ with an exponent $\alpha \simeq 0.6, \ldots, 0.7$ (see figure 10). Within the framework of simple diffusion models this B dependence is not understood, as for discrete jumps on a lattice $T_1 \propto B^2$ and for a liquid-like motion, $T_1 \propto B^{3/2}$, is predicted on the LTS [29]. We are thus faced with the problem that the values of $E_{\perp}$ and $\tau_{0\perp}$ are in accordance

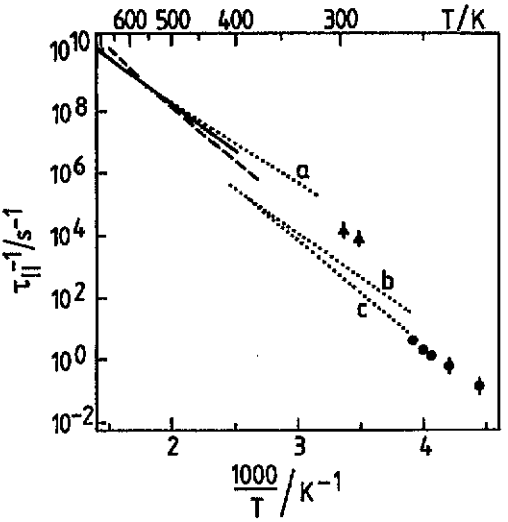

Figure 9. Arrhenius plot of $\tau_{\parallel}^{-1}$ determined from ^{8}Li SLR in T range I (solid line), ^{8}Li linewidths [21] (triangles), individual ^{8}Li transients $P(1)(t)$ (dots), ^{7}Li SLR [14] (broken line), and ionic conductivity $\sigma_{\parallel}$ ((a) from [5],(b),(c) from [16]).

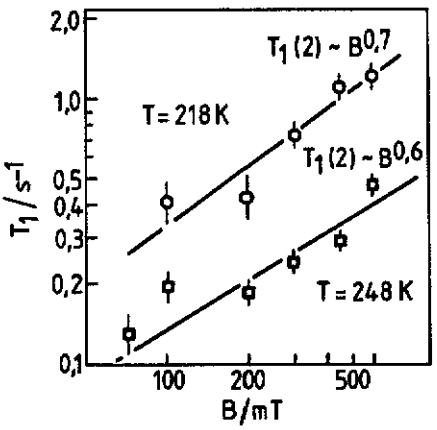

Figure 10. B dependence of $T_1(2)$.

with conductivity measurements (see figure 11) although they were inferred by means of the inappropriate spectral density function (22).

A possible starting point to explain the weak B dependence of $T_1(2)$ on the LTS is given by the treatment of paramagnetic SLR in the presence of spin diffusion carried out by Rohrschach [30], Khutsishvili [31] and Lowe and Tse [32]. Instead of spin diffusion, which is absent in β-NMR experiments, we assume here that the intralayer diffusion brings ^{8}Li(2) nuclei into the neighbourhood of fluctuating paramagnetic impurities, where they are depolarized efficiently. If a nucleus is completely depolarized during its residence time on a nearest neighbour site of a defect (distance a), which means that $\tau_{\perp} \gg T_1(a)$, we have what is generally called the diffusion-limited case. Neglecting low-dimensional effects of the intralayer diffusion one obtains within a three-dimensional continuum approximation, according to the authors cited above,

$$T_1^{-1}(2) = \frac{8\pi}{3} n_d D_{\perp}^{3/4} \left(\alpha_d \frac{\tau_d}{1 + \omega_L^2 \tau_d^2} \right)^{1/4} . \tag{25}$$

n_d, τ_d and α_d are the number of paramagnetic impurities per unit volume, their correlation time and the coupling strength of the interaction between them and the probe nuclei respectively. $D_{\perp}(2)$ is the Li(2) diffusion constant, i.e. $D_{\perp} = a^2/4\tau_{\perp}$. In the case $\omega_L \tau_d >> 1$ equation (25) predicts $T_1^{-1}(2) \propto \omega_L^{-1/2}$, which is close to the observed B dependence (figure 10). In order to get an estimation of the defect concentration n_d, we used equation (25) to fit the temperature dependence of $T_1^{-1}(2)$, assuming the Li(2)–Li(2) distance in a Li_2N layer to be $a = 0.213$ nm and the temperature-independent correlation time to be $\tau_d = 10^{-6}$ s. τ_d cannot be much shorter because of the condition $\omega_L \tau_d \gg 1$. Thus we obtained $E_{\perp} = 320(40)$ meV.

This is still in agreement with ionic conductivity measurements. If we then insert $\alpha_d \simeq \gamma_e^2\gamma_n^2\hbar^2 \simeq 10^{-32}$ cm^6 s^{-2} (γ_e and γ_n denote the gyromagnetic ratios of the electron and ^{8}Li spin) and $\tau_{0\perp} \simeq 10^{-12}$ s in (25) we finally obtain $n_d = 5\times10^{17}$ cm^{-3}, hence a rather small concentration of paramagnetic centres.

Thus we assume that the nominally pure Li_3N crystal contains a small amount of paramagnetic impurities, which in connection with the intralayer diffusion may cause the ^{8}Li(2) SLR. Evidence for the presence of paramagnetic impurities in Li_3N was found by Nishida *et al* [28], who detected a triplet EPR signal, from which a total spin concentration of 4.53×10^{-2} mol% could be determined. This is a factor of about 15 larger than that estimated for our hydrogen-rich sample. Additional NMR measurements showed that the relatively high concentration had a pronounced effect on the temperature dependence of the transverse ^{7}Li relaxation time T_2. Unfortunately the authors did not measure the frequency dependence of T_1, so that a comparison with our studies is not possible.

4.4. The ^{8}Li SLR in T range III ($T < 180$ K)

4.4.1. Measurements. The SLR in T range III was measured for the two orientations $\theta = 0°, 90°$ down to $T = 10$ K and in the magnetic field range $B = 37, \ldots, 600$ mT. Below $T = 200$ K the time constants $T_1(1)$ and $T_1(2)$ approach one another (figure 4) and from $T = 160$ K downwards a common relaxation time can be assumed, which was confirmed by the RF separation method at $T = 160$ K and $T = 100$ K. Furthermore, between 200 K and 160 K a transition to non-exponential relaxation occurs. The transients could be fitted quite well by the empirical function $P(t) \propto \exp[-(t/T_1)^\gamma]$ with an exponent γ in the range $0.2 \leqslant \gamma \leqslant 0.7$. The value of γ could not be accurately determined from the individual measurements of the polarization decay, so it had to be inferred from a SLR model, which will be presented in the next section. Using this model $\gamma = 1/3$ is predicted and this value was used as a fixed value to fit the measured transients in T range III. The B dependence of T_1 obtained from these fits is shown in figure 12. The SLR time obeys the empirical law $T_1 \propto B^\alpha$ with α varying from 0.8 to 1.4 over the T range investigated: 153 K to 50 K.

4.4.2. Discussion. The ^{8}Li SLR behaviour in T range III, i.e. non-exponential polarization decay together with a rather weak B dependence of T_1, is similar to that already found in Li-silicate and Li-borate glasses, where a $\exp[-(t/T_1)^{-1/2}]$ law was observed for the ^{8}Li transients and explained in the framework of statistically distributed relaxation centres (two-level systems?) in the glass network [33–35]. In the following we show that an analogous approach consistently explains the low-temperature relaxation of ^{8}Li in Li_3N. Here we tentatively assume that the relaxation centres can be identified with $(NH)^{--}$ dipoles reorienting randomly between certain directions in the Li_2N layers. Evidence for such a process was observed in measurements of the dielectric loss [36], infrared absorption [16] and acoustic absorption [7]. If matter and spin diffusion are absent, the influence of paramagnetic impurities on the ^{8}Li SLR is negligible unless their concentration exceeds the value given in section 4.3.4 by several orders of magnitude.

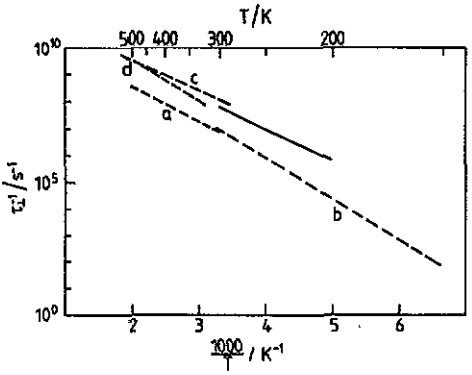

Figure 11. Arrhenius plot of the inverse correlation time $\tau_\perp^{-1}$ of intralayer diffusion in Li_3N crystals with approximately equal H contents from $^8Li(2)$ SLR in T range II (solid line) and from ionic conductivity $\sigma_\perp$ ((a),(b),(c),(d) from [5, 23, 36, 43]).

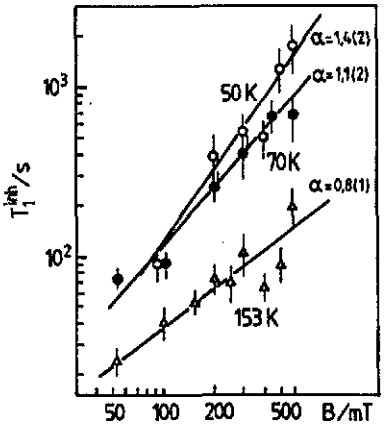

Figure 12. B dependence of T_1^{inh} obtained from fits with the functions $P(t) = P_0\exp[-(t/T_1{}^{inh})^{1/3}]$ (hydrogen-rich sample, $B \parallel c$).

Defects at the positions r_i fluctuating with correlation times τ_i will relax a reference spin at $r = 0$ with a rate [34]

$$\lambda = \sum_i a_0(r_0/r_i)^6 j(\omega, \tau_i) \tag{26}$$

where we neglected possible angular dependences of the coupling strength $a_0 r_0^6$. In the limit of vanishing spin and matter diffusion the transient of the total polarization is given by the inhomogeneous ensemble average [34]

$$P(t) = \langle \exp(-\lambda t) \rangle. \tag{27}$$

If the possible defect sites are confined to the Li_2N layers the average must take into consideration the layer structure of the defect configuration, which is only possible by means of a numerical calculation, so that (27) is no longer useful as a fit function for measured transients. We shall therefore restrict ourselves to the limiting case of a two-dimensional continuum approximation, i.e. we assume that the ^8Li nuclei are only influenced by defects in their own Li_2N layers (in the case of $^8Li(2)$) or by defects in neighbouring Li_2N layers (in the case of $^8Li(1)$).

In analogy to the three-dimensional (3D) continuum approximation given by [34], the ensemble average can be performed in the 2D case yielding [21]

$$P(t) = P_0 \exp[-(t/T_1^{inh})^{1/3}] \tag{28}$$

with the inhomogeneously averaged relaxation rate

$$1/T_1^{inh} = \pi^3 \Gamma(2/3)^3 r_0^6 a_0 \left(\int j(\omega, \tau)^{1/3} n_\tau(\tau)\, d\tau \right)^3. \tag{29}$$

Here $n_\tau(\tau)\, d\tau$ denotes the number of defects per unit area with correlation times τ in the interval $\tau, \ldots, \tau + d\tau$. We now consider the last formula in order to see

whether it is able to predict the measured B dependence, i.e. $T_1^{inh} \propto B^\alpha$ with α close to 1.0. Assuming $j(\omega,\tau) = 2\tau/(1+(\omega\tau)^2)$, we note firstly that if all relaxation centres have the same correlation time τ_d, i.e. $n_\tau(\tau) = n_d\delta(\tau-\tau_d)$ a BPP formula for $1/T_1^{inh}$ is obtained that is unsuited to allowing for the variation of T_1^{inh} with B. Hence we assume, that $n_\tau(\tau)$ represents a broad distribution of correlation times. Then (29) still contains the limiting BPP cases $T_1^{inh} \propto B^2$ and $T_1^{inh} \propto B^0$ for low and high temperatures respectively, but there exists a more or less broad intermediate T range where $T_1^{inh} \propto B^\alpha$ with $0 < \alpha < 2$ can be observed. For these temperatures we use an approximation described by [34], where $n_\tau(\tau)d_\tau$ is replaced by the corresponding energy distribution $n_E(E)\,dE$. τ and E are connected via an Arrhenius law $\tau = \tau_0\exp(E/kT)$. If $n_E(E)$ is a slowly varying function of E, (29) can be approximated by

$$1/T_1^{inh} = \frac{\pi^3}{8}\left(\frac{\Gamma(2/3)\Gamma(1/6)^2}{\Gamma(1/3)}\right)^3 \tau_0^6 a_0 \frac{(kT)^3}{\omega} n_E(E')^3 \tag{30}$$

where E' is the maximum of $j(\omega,\tau_0\exp(E/kT))$ considered as a function of E. One then gets

$$E' = kT\ln(1/\omega\tau_0). \tag{31}$$

Hence T_1^{inh} is proportional to ω if one neglects the weak logarithmic ω dependence of E'.

It should be mentioned here that a 3D *continuum model predicts* [34]

$$P(t) = P_0\exp\left(-[t/(T_1^{inh})_{3D}]^{1/2}\right) \tag{32}$$

with

$$1/(T_1^{inh})_{3D} \propto \frac{(kT)^2}{\omega} n_E(E')^2. \tag{33}$$

The function (32) can also be used to fit the ^{8}Li transients. In this case, however, a B dependence of $(T_1^{inh})_{3D} \propto B^\alpha$ with $\alpha \simeq 0.5,\ldots,0.8$ is obtained, which contradicts (33). The model of a two-dimensional defect configuration thus seems to describe the ^{8}Li SLR behaviour in T range III more appropriately.

By inspection of figure 12 we see that $T_1^{inh} \propto \omega^\alpha$ with $\alpha \simeq 1$ is fulfilled near $T \simeq 70$ K. Obviously there is a trend to exponents $\alpha > 1$ for $T < 70$ K and $\alpha < 1$ for $T > 70$ K. The approximations used to arrive at the relation (30) should thus be admissible within the approximate limits $T_{min} \simeq 50$ K and $T_{max} \simeq 150$ K. In this T range α varies between 0.8 and 1.4.

According to (30) the energy distribution $n_E(E')$ of the relaxation centres is given by

$$n_E(E') \propto \left(\frac{\omega}{T_1^{inh}T^3}\right)^{1/3}. \tag{34}$$

In figure 13 $[\omega/(T_1^{inh}T^3)]^{1/3}$ is plotted against E', which was determined from equation (31) with $\tau_0 = 10^{-13}$ s. The ordinate is proportional to $n_E(E')$ in the

energy interval (60–180 meV) which is equivalent to the T range $T_{min}, \ldots, T_{max}$. Beyond this interval the validity of (30) or (34) is not ensured and reliable values for $n_E(E')$ cannot be obtained. Moreover, above $E' \simeq 205$ meV, the influence of the intralayer diffusion produces a fictitious increase of $n_E(E')$. Measurements for the orientation $B \parallel c$ as well as for $B \perp c$ yield about the same energy distribution, so that the neglect of angle dependent terms in (26) is justified. Unexpectedly, the different H contents of the samples have no influence on $n_E(E')$. The question of whether the relaxation centres are connected with the hydrogen impurities thus remains unclear for the present.

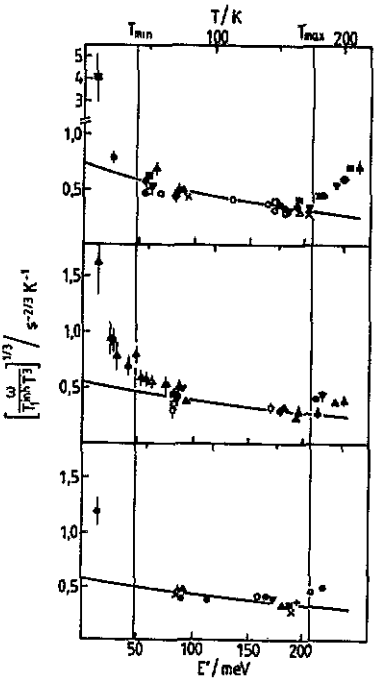

Figure 13. Energy distribution $n_E(E')$ of the relaxation centres. The ordinates $[\omega/(T_1^{inh}T^3)]^{1/3}$ are proportional to n_E between the limits T_{min} and T_{max}. The symbols correspond to the B values given below. The lines are extrapolations by means of an exponential function. +: 37 mT; ×: 50 mT; ∗ : 100 mT; ▲ : 125 mT; △ : 150 mT; ▽ : 200 mT; ● : 250 mT; • : 300 mT; ■ : 400 mT; □ : 500 mT; o : 600 mT.

From the results of figure 13 a rough estimate of the defect concentration

$$n_d = \int_0^\infty n_E(E')\,dE' \tag{35}$$

can be made if the coupling strength $a_0 r_0^6$ entering into equation (26) is known. Assuming for simplicity that the relaxation centre is a point charge we have a quadrupolar SLR mechanism, where $a_0 r_0^6$ is of the order of $(e^2Q/h)^2 = 5 \times 10^{-35}$ cm^6 s^{-2}. For real cases, $a_0 r_0^6$ should not differ from this value by many orders of magnitude, so that we allow it to vary in a range, say, from 10^{-33} to 10^{-36} cm^6 s^{-2}. This yields a defect concentration of $n_d = (3, \ldots, 25) \times 10^{13}$ cm^{-2} or a number ratio of defects per Li(2) lattice site $N_d/N(2) = 1, \ldots, 8$ % if the data between T_{min} and T_{max} are extrapolated by means of an empirical exponential function (continuous line in figure 13). These values are close to typical Li(2)-vacancy and hydrogen concentrations inferred from x-ray structure [37] and infrared absorption [16] measurements, respectively.

4.4.3. Conclusion. The interpretation of the low-temperature relaxation of ^8Li in Li_3N in the framework of two-dimensionally distributed relaxation centres with a broad distribution of activation energies requires knowledge of the microscopic nature of these defects, which obviously bear strong ressemblance to two-level systems (TLS) in glasses. Indeed several low-temperature properties of Li_3N crystals have been attributed to the influence of TLS. So the temperature dependence of the specific heat [38], the velocity of sound [7, 39] and the dielectric constant [7, 36] below $T = 6$ K are explicable by TLS with a constant energy distribution between $E = 0$ and $E = 3, \ldots, 11$ meV depending on the H content. Baumann *et al* [7] suggest identifying the TLS with a proton tunnelling between neighbouring N ions. However, all these effects occur far below $T = 10$ K, so that the N–H tunnel system is unlikely to be responsible for the ^8Li SLR in the T range 10,...,170 K. The maximum energy cited above is also far below the energy range of figure 13, which extends up to about 200 meV.

An alternative is to start with measurements of the infrared [16] and ultrasonic [7] absorption as well as from the dielectric loss [36] for $T > 10$ K. The IR absorption resonance of the N–H vibration shows a fine structure, which is explicable by different configurations of the $(NH)^{--}$ dipoles with associated Li^+ vacancies. Reorientational processes between these configurations with different activation energies would lead to fluctuations of the electric fields at ^8Li sites with a distribution of correlation times τ and would entail quadrupolar SLR.

The result for the defect concentration n_d, however, remains unresolved. An agreement with typical hydrogen concentrations is certainly found, but contrary to IR absorption measurements, which reveal a ratio of 5:1 for the H contents of the samples studied here, the ^8Li SLR yields a sample-independent defect concentration. If the identification of the relaxation centres with fluctuating $(NH)^{--}$ dipoles is, however, maintained (impurities other than hydrogen were not found in Li_3N) a concentration-independent energy distribution $n_E(E')$ in the range $E' = 60, \ldots, 180$ meV has to be assumed. Different $n_E(E')$ values for the two samples should then show up outside this energy range. The situation here is probably analogous to the one for the N–H tunnel system cited above. From the T dependence of the ultrasonic velocity between 30 mK and 3 K Baumann *et al* [39] found a constant energy distribution of the TLS states, which remained unchanged even when the hydrogen concentration was varied by a factor of 40.

Acknowledgments

We are grateful to W Kress for the loan of the crystal and for characterizing measurements and to W Kress, R Messer, and A Seeger for helpful comments. We thank the Institut Laue Langevin, Grenoble, and the Institut für Festkörperforschung, Forschungszentrum Jülich, for hospitality. This work was sponsored by the Bundesministerium für Forschung und Technologie.

Appendix. The spectral densities of the interlayer diffusion

We consider a mobile probe nucleus jumping between lattice sites i, where electric field gradients with EFG tensor components $V_2^m(i)$ are present. If their average

taken over all accessible sites $\bar{V}_2^m = \sum n(i) V_2^m(i)$ with the statistical weights $n(i)$ ($\sum n(i) = 1$) does not vanish, the Hamiltonian reads

$$\mathcal{H} = \mathcal{H}_0 + \mathcal{H}_1(t) \tag{A.1}$$

with

$$\mathcal{H}_0 = -\omega_L I_z + \sum_{m=-2}^{2} \bar{V}_2^m Q_2^{-m} \tag{A.2}$$

$$\mathcal{H}_1 = \sum_{m=-2}^{2} [V_2^m(t) - \bar{V}_2^m] Q_2^{-m}. \tag{A.3}$$

For the definition of the quadrupole tensor components Q_2^m and the EFG tensor components V_2^m see e.g. [40]. The static part $\mathcal{H}_0$ leads in the case of ^{8}Li in Li_3N to the NMR spectrum of figure 3 with the averaged coupling constant $e^2\bar{q}Q/h$ of a few kHz. The fluctuating part $\mathcal{H}_1(t)$ contains the time dependent $V_2^m(t)$, which take on the values $V_2^m(i)$ at a random rate. The correlation functions $G_1(t)$ and $G_2(t)$ governing the quadrupolar SLR can then be defined as

$$G_m(t) = \sum_{i,j} n(i)[V_2^m(i) - \bar{V}_2^m][V_2^{-m}(j) - \bar{V}_2^{-m}]P(i,j;t) \qquad m = 1,2. \tag{A.4}$$

$P(i,j;t)$ denotes the probability for a nucleus to move from i to j in the time interval t. Introducing the jump probabilities per unit time W_{ij} for a transition from site i to site j, the functions $P(i,j;t)$ can be calculated by use of the master equations (cf. [41])

$$\dot{P}(i,j;t) = \sum_{k,k\neq j} [W_{kj}P(i,k;t) - W_{jk}P(i,j;t)] \tag{A.5}$$

with the initial conditions $P(i,j;0) = \delta_{ij}$.

For a jump process involving only two inequivalent lattice sites, designated by 1 and 2, (A.5) is easily solved . From (A.4), (A.5) and the condition of detailed balance:

$$n(1)W_{12} = n(2)W_{21} \tag{A.6}$$

we get for the correlation functions

$$G_m(t) = n(1)n(2)[V_2^m(1) - V_2^m(2)]^2 \exp(-t/\tau) \qquad m = 1,2 \tag{A.7}$$

with $\tau = (W_{12} + W_{21})^{-1}$ and after a Fourier transformation the spectral densities

$$J_m(\omega,\tau) = n(1)n(2)[V_2^m(1) - V_2^m(2)]^2 \frac{2\tau}{1+\omega^2\tau^2} \qquad m = 1,2. \tag{A.8}$$

We now consider the special case of the interlayer diffusion in Li_3N. For $B \parallel c$ we have $V_2^m(i) = 1/2eq(i)\delta_{m0}$. For an arbitrary angle θ between B and c the $V_2^m(i)$ transform according to

$$V_2^m(i,\theta) = \sum_{m'=-2}^{2} d_{m'm}^2(\theta) V_2^m(i) \tag{A.9}$$

with the rotational matrix elements $d^2_{m',m}(\theta)$ [42]. Furthermore, the statistical weights are $n(1) = 1/3$, $n(2) = 2/3$ and the jump probabilities can be set to $W_{12} =: W$, $W_{21} =: W/2$, which follows immediately from the ratio $n(2)/n(1) = 2$ and the condition (A.6).

From (A.8) and (A.9) we then obtain the spectral densities of the interlayer diffusion

$$J_1(\omega, \tau_\parallel) = \frac{1}{12}[eq(1) - eq(2)]^2 \sin^2\theta \cos^2\theta \frac{2\tau_\parallel}{1 + \omega^2\tau_\parallel^2}$$
$$J_2(\omega, \tau_\parallel) = \frac{1}{48}[eq(1) - eq(2)]^2 \sin^4\theta \frac{2\tau_\parallel}{1 + 4\omega^2\tau_\parallel^2} \tag{A.10}$$

where the correlation time $\tau_\parallel$ is given by

$$\tau_\parallel = (W_{12} + W_{21})^{-1} = (\tfrac{3}{2}W)^{-1}. \tag{A.11}$$

References

[1] Zintl E and Brauer G 1935 *Z. Elektrochem.* **41** 102
[2] Krebs H 1956 *Acta Crystallogr.* **9** 95
[3] Suchet J P 1961 *Acta Crystallogr.* **14** 651
[4] Rabenau A 1982 *Solid State Ionics* **6** 277
[5] v Alpen U, Rabenau A and Talat G H 1977 *Appl. Phys. Lett.* **30** 621
[6] Schulz H and Thiemann K H 1979 *Acta Crystallogr.* **A35** 309
[7] Baumann T, von Schickfuß M, Hunklinger S and Jäckle J 1980 *Solid State Commun.* **35** 587
[8] Ackermann H, Dubbers D and Stöckmann H-J 1978 *Advances in Nuclear Quadrupole Resonance* vol 3, ed J A S Smith (London: Heyden) pp 1–66
[9] Ackermann H, Heitjans P and Stöckmann H-J 1983 *Hyperfine Interactions of Radioactive Nuclei (Topics in Current Physics 31)* ed J Christiansen (Berlin: Springer) p 291
[10] Heitjans P 1986 *Solid State Ionics* **18/19** 50
[11] Heitjans P, Faber W and Schirmer, A 1991 *J. Non-Cryst. Solids* **131–133** 1053
[12] Brinkmann D, Freudenreich W and Roos J 1978 *Solid State Commun.* **28** 233
[13] Brinkmann D, Mali M, Roos J, Messer R and Birli H 1982 *Phys. Rev.* B **26** 4810
[14] Messer R, Birli H and Differt K 1981 *J. Phys. C: Solid State Phys.* **14** 2731
[15] Schönherr E, Müller G and Winkler E 1978 *J. Crystal Growth* **43** 469
[16] Wahl J 1979 *Solid State Commun.* **29** 485
[17] Stöckmann H-J, Dubbers D, Grupp M, Grupp H, Ackermann H, and Heitjans P 1974 *Z. Phys.* **269** 47
[18] Dubbers D, Dörr K, Ackermann H, Fujara F, Grupp H, Grupp M, Heitjans P, Körblein A and Stöckmann H-J 1977 *Z. Phys.* A **282** 243
[19] Differt K and Messer R 1980 *J. Phys. C: Solid State Phys.* **13** 717
[20] Blaha P, Schwarz K and Herzig P 1985 *Phys. Rev. Lett.* **54** 1192
[21] Bader B 1986 *Thesis* University of Marburg
[22] Bader B, Heitjans P, Ackermann H, Freiländer P, Kiese G, Schirmer A, Stöckmann H-J and Van der Marel C 1985 *Ann. Phys., Lpz* **42** 169
[23] Hooper A, Lapp T and Skaarup S 1979 *Mat. Res. Bull.* **14** 1617
[24] Bloembergen N, Purcell E M and Pound R V 1948 *Phys. Rev.* **48** 679
[25] Körblein A, Heitjans P, Stöckmann H-J, Fujara F, Ackermann H, Buttler W, Dörr K and Grupp H 1985 *J. Phys. F: Met. Phys.* **15** 561
[26] Brinkmann D Private communication
[27] Bader B, Heitjans P, Ackermann H, Fujara F, Kiese G, Stöckmann H-J and Van der Marel C 1983 *Hyperfine Interact.* **15/16** 593

[28] Nishida K, Asai T and Kawai S 1983 *Solid State Commun.* **48** 701
[29] Bjorkstam J L and Villa M 1980 *Magn Res. Rev.* **6** 1
[30] Rohrschach H E 1964 *Physica* **30** 38
[31] Khutsishvili G R 1956 *Proc. Inst. Phys. Acad. Sci. Georgia (USSR)* **4** 3
[32] Lowe I J and Tse D 1968 *Phys. Rev.* **166** 279
[33] Heitjans P, Bader B, Stöckmann H-J, Dörr K, Kiese G, Ackermann H, Freiländer P, Müller-Warmuth W and Meise-Gresch K 1983 *Hyperfine Interact.* **15/16** 597
[34] Stöckmann H-J and Heitjans P 1984 *J. Non-Cryst. Solids* **66** 501
[35] Schirmer A, Heitjans P, Bader B, Freiläner P, Stöckmann H-J and Ackermann H 1991 *J. Phys.: Condens. Matter* **3** 4323
[36] Wahl J and Holland U 1978 *Solid State Commun.* **27** 237
[37] Schulz H and Schwarz K 1978 *Acta Crystallogr.* A **34** 999
[38] Gmelin E and Guckelsberger K 1981 *J. Phys. C: Solid State Phys.* **14** L21
[39] Baumann T, von Schickfuß M and Hunklinger S 1981 *Physica* B **108** 1267
[40] Abragam A 1961 *The Principles of Nuclear Magnetism* (Oxford: Clarendon)
[41] Barber M N and Ninham B W 1970 *Random and Restricted Walks* (London: Gordon and Breach)
[42] Rose M E 1957 *Elementary Theory of Angular Momentum* (New York: Wiley)
[43] Bell M F, Breitschwert A and von Alpen U 1981 *Mat. Res. Bull.* **16** 267